

Prediction of Flows about Forebodies at High-Angle-of-Attack Dynamic Conditions

C.P. van Dam and S. Saephan

Department of Mechanical and Aeronautical Engineering
University of California, Davis
One Shields Avenue
Davis, CA 95616-5294
USA

C.M. Fremaux

Vehicle Dynamics Branch
NASA Langley Research Center
Mail Stop 343
Hampton, VA 23681-2199
USA

T. DalBello

Ohio Space Institute, ICOMP
NASA Glenn Research Center
Lewis Field, MS 5-11
Cleveland, OH 44135
USA

Abstract

A Reynolds-average Navier Stokes method developed for rotorcraft type of flow problems is applied for predicting the forces and moments of forebody models at high-angle-of-attack dynamic conditions and for providing insight into the flow characteristics at these conditions. Wind-tunnel results from rotary testing on generic forebody models conducted by NASA Langley and DERA are used for comparison. This paper focuses on the steady-state flow problem.

Introduction

The stability and control at post-stall maneuvering flight conditions are of major concern in the design of advanced agile airplanes. At these flight conditions the flows about this type of aircraft tend to be unsteady and the aerodynamic forces and moments show strong nonlinear variations with rotation rates. During the development process of these airplanes, numerous hours are spent testing scaled models in ground facilities with complex special purpose equipment to determine the dynamic stability and control characteristics. Much of this testing is conducted using sub-scale models of simplified geometry at low Reynolds numbers. In addition to this largely experimental approach, potential-flow type of prediction methods including empirical viscous corrections are being used to predict loads on forebodies under separated-flow conditions. However, the sensitivity of the forces and moments to geometric detail and Reynolds number makes these (semi-)empirical approaches to predict the dynamic characteristics at full-scale high-angle-of-attack conditions a challenging task.

In the mid-1990s, rotary balance experiments were conducted on square and circular ogive forebodies at angles of attack of 60 and 90 degrees over a range of Reynolds numbers (based on the body diameter/width, D , and freestream velocity, U_∞) from 0.08×10^6 to 2.25×10^6 (Refs. 1 and 2). Figure 1 depicts the two forebody models with square and circular cross sectional shape. The purpose of these experiments was to determine the effects of Reynolds number, angular velocity, and geometric shape on

Report Documentation Page				Form Approved OMB No. 0704-0188	
Public reporting burden for the collection of information is estimated to average 1 hour per response, including the time for reviewing instructions, searching existing data sources, gathering and maintaining the data needed, and completing and reviewing the collection of information. Send comments regarding this burden estimate or any other aspect of this collection of information, including suggestions for reducing this burden, to Washington Headquarters Services, Directorate for Information Operations and Reports, 1215 Jefferson Davis Highway, Suite 1204, Arlington VA 22202-4302. Respondents should be aware that notwithstanding any other provision of law, no person shall be subject to a penalty for failing to comply with a collection of information if it does not display a currently valid OMB control number.					
1. REPORT DATE 00 MAR 2003		2. REPORT TYPE N/A		3. DATES COVERED -	
4. TITLE AND SUBTITLE Prediction of flows about Forebodies at High-Angle-of-Attack Dynamic Conditions				5a. CONTRACT NUMBER	
				5b. GRANT NUMBER	
				5c. PROGRAM ELEMENT NUMBER	
6. AUTHOR(S)				5d. PROJECT NUMBER	
				5e. TASK NUMBER	
				5f. WORK UNIT NUMBER	
7. PERFORMING ORGANIZATION NAME(S) AND ADDRESS(ES) NATO Research and Technology Organisation BP 25, 7 Rue Ancelle, F-92201 Neuilly-Sue-Seine Cedex, France				8. PERFORMING ORGANIZATION REPORT NUMBER	
9. SPONSORING/MONITORING AGENCY NAME(S) AND ADDRESS(ES)				10. SPONSOR/MONITOR'S ACRONYM(S)	
				11. SPONSOR/MONITOR'S REPORT NUMBER(S)	
12. DISTRIBUTION/AVAILABILITY STATEMENT Approved for public release, distribution unlimited					
13. SUPPLEMENTARY NOTES Also see: ADM001490, Presented at RTO Applied Vehicle Technology Panel (AVT) Symposium held inLeon, Norway on 7-11 May 2001, The original document contains color images.					
14. ABSTRACT					
15. SUBJECT TERMS					
16. SECURITY CLASSIFICATION OF:			17. LIMITATION OF ABSTRACT UU	18. NUMBER OF PAGES 16	19a. NAME OF RESPONSIBLE PERSON
a. REPORT unclassified	b. ABSTRACT unclassified	c. THIS PAGE unclassified			

the aerodynamic characteristics of the forebodies. These tests were unique in so far that this was the first time that surface pressure distributions were measured under dynamic conditions in a pressurized wind tunnel. A second objective of these experiments was to provide a database for the development/validation of high-angle-of-attack computational methods. This database forms the basis for the computational investigation.

The numerical simulation of rotary aerodynamics is only in its infancy. Inviscid methods and viscous/inviscid interaction methods tend to be inapplicable because of the strong viscous effects and the large regions of flow separation that occur at high-angle-of-attack conditions. Also, methods based on the Euler equations only predict vortex formation originating from flow separation at sharp edges and ignore the vortices that originate from flow separation at smooth surfaces. At present, the only viable computational approach for the prediction of aircraft dynamics at high angles of attack is based on the time-dependent three-dimensional Reynolds-averaged Navier-Stokes (RaNS) equations. Unfortunately much of the developments in computational fluid dynamics (CFD) have concentrated on static problems, such as the computation of lift and drag of aircraft at stationary conditions. Relatively few researchers have explored the application of three-dimensional CFD methods to aircraft dynamic problems.

A few studies provide approaches to deal with body motion in CFD simulations including Kandil & Chuang (Ref. 3), Weinacht, Sturek et al (Refs. 4-7), Chaderjian & Schiff (Ref. 8), Ahmad & Duque (Ref. 9), Limache & Cliff (Ref. 10), and Park & Green (Ref. 11). Kandil & Chuang (Ref. 3) studied the flow about an oscillating delta wing at supersonic conditions using the RaNS equations in conical form. Weinacht, Sturek et al (Refs. 4-7) analyzed the damping characteristics of various motions (including coning motion) of projectiles at supersonic conditions using a parabolized Navier-Stokes method. Chaderjian & Schiff (Ref. 8) analyzed the wing-rock problem of delta wings at high angle of attack using a single-grid technique whereas Ahmad & Duque (Ref. 9) analyzed the flow around a rotating helicopter rotor using a more general overset grid technique. Through various enhancements of the RaNS solver OVERFLOW, the latter methodology has been developed further by the Army/NASA rotorcraft group at Ames Research Center. These enhancements have made it feasible to efficiently simulate the rotary flows over forebodies without the need for extensive modifications of flow solvers developed for static problems. Limache & Cliff (Ref. 10) analyzed rotary stability derivatives using an ingenious sensitivity equation method and applied this scheme to solve the pitch-rate derivatives for airfoils at inviscid flow conditions. Park & Green (Ref. 11) modified the general purpose RaNS solver CFL3D to compute stability derivatives for a various configurations including a complete airplane.

In the next section the forebody models as well as the experimental setup used to generate the database are discussed, followed by a brief discussion of the rotorcraft version of OVERFLOW and the computational grids on which the solutions were obtained. Computational results are presented for the circular and square ogives at steady rotary conditions and these results are compared against the experimental findings.

Geometry of Forebody Models and Test Setup

The rotary flow experiments were part of a cooperative effort between NASA Langley and DERA (Defense Evaluation & Research Agency) and were conducted in the United Kingdom in the atmospheric 13 ft \times 9 ft wind tunnel at Bedford and in the pressurized 8 ft \times 6 ft wind tunnel at Farnborough, utilizing the DERA rotary balance apparatus. These wind tunnels provided a freestream Mach number range from 0.024 to 0.21 and a Reynolds number range from 0.15 to 4.5 million per foot for these tests. The sketch in Fig. 2 depicts the test setup as it was numerically simulated in the present investigation.

Detailed descriptions of the forebody models are presented by Pauley et al (Ref. 1) and Dunham (Ref. 2) and sketches of the models are shown in Fig. 1. As shown in Fig. 1, one set of model configurations has a square cross sectional shape with rounded corners whereas the second set of models has a circular cross sectional shape. The detachable aftbodies have a hemispherical shape. The detachable forebodies have either a hemispherical or a 2.0D ogive shape. Although both the square and the circular configurations

were wind-tunnel tested with the hemispherical as well as the ogive forebodies, only the configurations with the ogive forebody shape are considered in this computational study. Detailed surface measurements were conducted for both ogive forebody models and were used to create the surface grids. Both forebodies turn out to be slightly asymmetric.

The ogive models have six rows of pressure taps in the forebody and two rows of pressure taps in the aft section for a total of 254 taps. Each model has a length, b , of 36 in. and a maximum diameter/width, D , of 6 in. The forebody has a length of 12 in. and the hemispherical aftbody a length of 3 in. Each model is mounted to the internal force-and-moment strain gage balance which in turn is connected to the rotary apparatus via a sting located 18 in. from the nose. Note that neither the sting nor any other rotary-balance equipment is included in the computational model at this point in the study.

Flow Solver

The Reynolds-average Navier Stokes (RaNS) method used to solve the flows about forebodies at high-angle-of-attack dynamic conditions is based on version 1.8 of OVERFLOW (Ref. 12). OVERFLOW has been developed by Buning et al for problems involving fixed-wing aircraft (Ref. 12). It solves the governing flow equations on structured overset grids. The reasons for selecting this code are multifold. First, the code is well documented and supported by Buning and his colleagues. Second, the code uses the overset or Chimera grid approach to facilitate the solution of flows involving complex geometries. Third, researchers of the Army/NASA Rotorcraft Division at the Ames Research Center have enhanced the basic OVERFLOW code by adding rotorcraft-specific capabilities. The enhancements that facilitate the solution of rotorcraft type of flow problems include rotational rigid-blade motion, dynamic interpolation of solution quantities between rotating and non-rotating grids (Ref. 13), and a source-term formulation to allow steady flow solutions of the rotor-in-hover problem (Refs. 14-16). In the present study, particularly this last feature turned out to be very useful and resulted in significant savings in computing time.

The resulting Navier-Stokes equations for a rotating body in a compressible flow can be written as follows (Ref. 16):

$$\frac{\partial Q}{\partial t} + E(Q) = V(Q) + R(Q) \quad (1)$$

where $Q = [p, \rho u, \rho v, \rho w, e]^T$ is the solution vector of conserved variables for the mass, momentum, and energy equations. Also in Eq. (1), the variable $E(Q) = \frac{\partial E_i}{\partial x_i}$ represents the convective operator, $V(Q) = \frac{\partial V_i}{\partial x_i}$ represents the thin-layer viscous operator, and $R(Q) = [0, \rho v \Omega, -\rho u \Omega, 0, 0]^T$ represents the source term to allow solution of the rotary flow problem using the steady formulation of the equations. Note that this formulation fixes rotation at constant angular velocity, Ω , to that about the z-axis (Fig. 2).

OVERFLOW provides a wide choice of algorithms to solve the governing equations. The results presented in this paper are conducted fully turbulent using the Baldwin-Lomax turbulence model (Ref. 17) or the Spalart-Allmaras turbulence model (Ref. 18). In all cases, central differencing is used on the right-hand-side of the equations. The LU-SGS scheme is used on the left-hand side. This scheme was selected because it had been previously tested with the source term in place for steady flow conditions (Ref. 16). The second- and fourth-order dissipation terms are set at the default settings for subsonic viscous flow problems; 0.0 and 0.04, respectively.

Computational Grids

A total of 22 axial stations supplied the information for the surface grid generation for each configuration. The surface grids for the two configurations were generated with the software package OVERGRID (Refs. 18, 19). OVERGRID is a graphical user interface for communicating with a wide variety of grid generation modules. Although it is tailored for overset grids, only single grids were used to simulate the

flows over the circular and square forebody models. Each surface grid consists of 181 equidistant points circumferentially at a total of 130 and 131 axial stations for the circular and square ogive, respectively.

The volume grids for the ogive forebody models were also generated using OVERGRID. For both models the outer boundary of the grid was specified at 50 body diameters. The first four grid points off the surface have a constant spacing of $0.00033D$. Starting at grid point number five, the grid is stretched at a constant factor of approximately 1.25 resulting in a total number of grid points of 54. Close-ups of the grids for the two models are shown in Fig. 3. These grids were initially developed for $Re_D = 2.0 \times 10^5$. Extensive validation studies for laminar flow over a circular cylinder resulted in grid independent solutions and excellent agreement with experimental data in terms of Strouhal number and average drag coefficient. Further grid refinement may be required for the higher Reynolds number turbulent flow cases considered here.

Results

Simulations were conducted for both the circular ogive and the square ogive. The aerodynamic coefficients are based on freestream dynamic pressure $\gamma p_\infty M_\infty^2/2$, area $Db = 216 \text{ in}^2$ for the forces and moments, and length D for the moments.

The circular ogive at $\alpha = 60^\circ$, $Re_D = 2.08 \times 10^6$, $M_\infty = 0.21$, $\Omega b/(2U_\infty) = -0.20$ was analyzed using the steady formulation of the Reynolds-averaged Navier Stokes equations and fully turbulent flow. The turbulence model used was the algebraic Baldwin-Lomax model (Ref. 17). Figures 4 and 5 depict the convergence characteristics in terms of the L2-norm, the normal force coefficient, the side force coefficient, and the yawing moment coefficient. After 9000 iteration steps, the residual in terms of the L2-norm is reduced by approximately three-orders of magnitude and the computed force and moment coefficients begin to level off. The normal force coefficient converges to a value of -0.33, the side force coefficient to a value of 0.18, and the yawing moment coefficient to a value of 0.027. For this case, the side force and moment results based on the measurements in the pressurized 8 ft \times 6 ft wind tunnel at Farnborough are reported in Ref. 1. According to Ref. 1, the experimental results indicate a side force coefficient of 0.18 and a yawing moment coefficient of 0.012; i.e., excellent agreement is obtained for the side force whereas the yawing moment is significantly overpredicted. In Figs. 6 and 7 the measured and predicted forebody pressure distributions are compared. No pressures were measured near the nose tip and hence the pressures in this region are left undefined. The experimental surface pressures were determined using as a reference the pressure in a container located inside the ogives. During the wind tunnel tests, problems were encountered correlating this reference pressure to the freestream pressure. This may explain the consistently high experimental pressures and the resulting discrepancy between experimental and computed pressure distributions. The shift in the experimental results is particularly apparent in the flow attachment region where C_p values in excess of unity are indicated. Based on the low freestream Mach number ($M_\infty = 0.21$) and the low rotational velocity ($\Omega b/(2U_\infty) = -0.20$), pressure coefficients much greater than unity would not be expected. However, overall the pressure distributions show good agreement with both distributions depicting the skewness in the distribution under the influence of the angular velocity component. Figure 8 shows the axial vorticity component at four body stations. Figure 8b and 8e depict the axial vorticity contours for the forebody and the aftbody, respectively, with both plots clearly showing the rotational effect. Figures 8c and 8d depict the vorticity distribution near the axis of rotation and hence, these distributions don't show as much skewness.

The square ogive at nearly identical conditions ($\alpha = 60^\circ$, $Re_D = 2.09 \times 10^6$, $M_\infty = 0.21$, $\Omega b/(2U_\infty) = -0.20$) was analyzed using the identical formulation and turbulence model. For this case, the convergence characteristics are very similar to those for the circular ogive. The normal force coefficient converges to a value of -0.39, the side force coefficient to 0.17, and the yawing moment coefficient to 0.29. Again, the side force and yawing moment results based on the measurements in the pressurized 8 ft \times 6 ft wind tunnel at Farnborough are reported in Ref. 1. According to Ref. 1, the experimental results indicate a side force coefficient of 0.16 and a yawing moment coefficient of 0.036. Hence good agreement is obtained

for the side force whereas the yawing moment is overpredicted. In Figs. 9 and 10 the measured and predicted forebody pressure distributions are compared. Note that the color contour scale is as defined in Fig. 6. Except for the beforementioned shift in the experimental data, the pressure distributions show good agreement with both distributions depicting the skewness in the distribution under the influence of the angular velocity component. The relatively good agreement in the forebody pressure distributions and, hence, forebody forces & moments raises the question as to what is causing the overprediction of the yawing moment.

The discrepancy between the measured and computed values for the yawing moment coefficient motivated us to rerun this case with the Spalart-Allmaras (S-A) one-equation turbulence model (Ref. 18) instead of the Baldwin-Lomax (B-L) algebraic model (Ref. 17). Murman & Chaderjian (Ref. 21) report slightly more accurate results when the former model was used to study the separated flow about a tangent-ogive cylinder at high angles of attack. In Fig. 11 the forebody pressure distributions and axial vorticity distributions are compared. The normal force coefficient is shown to converge to a value of -0.56, the side force coefficient to a value of 0.21, and the yawing moment coefficient to a value of 0.31. The increase in the magnitude of the normal force coefficient (-0.39, B-L versus -0.56, S-A) is in line with the findings of Murman & Chaderjian (Ref. 21) for the ogive cylinder at high angles of attack. However, the yawing moment coefficient (0.29, B-L versus 0.31, S-A) is much less affected by the choice of turbulence model and remains inconsistent with the wind-tunnel results.

Discussion

The computational results for the high-Reynolds-number rotary flow cases presented in the previous section show good agreement with the experimental results in terms of the forebody pressure distributions, normal force coefficients, and side force coefficients. The agreement for the yawing moment coefficient is less consistent. Keeping in mind that aerodynamic moments are as or more difficult to predict than aerodynamic drag, it is appropriate to refer to Ref. 22 for a list of possible reasons for this discrepancy. As pointed out in Ref. 22, the accuracy of CFD-based force & moment predictions depends on a large number of factors including geometry representation, grid size/density, flow solver, convergence level, transition prediction, and turbulence modeling.

Detailed surface measurements of the forebodies were taken to obtain an accurate representation of the ogive geometries. However, the sting (see Fig. 2) which connects the model to the rotary apparatus may have a noticeable effect on the flow development over the mid- and aft-body. At this point the sting is not modeled. This device is expected to affect the vortical flow development along the aft part of the body. This could explain the apparent relatively good agreement between the predicted and measured pressures on the forebody and at the same time the relatively poor agreement in the yawing moment.

Grid size/density is nearly always an issue for 3-D viscous flow simulations. Although the speed and memory size of computers have increased, allowing the solution of larger flow problems, the need to reduce turn-around as well as CPU time and, hence, cost, pushes users to obtain solutions on smaller grids. Also in this study a tradeoff was made between grid size and computational cost with the current grid size encompassing approximately 1.3 million points with 130 points axially, 181 points circumferentially, and 54 points normally. A grid spacing of $\Delta\phi = 1^\circ$ is required in the circumferential direction to more accurately capture the flow separation phenomena and ensuing vortical flow along the lee side of the body. Also the initial normal spacing, $\Delta y_o = 3.3 \times 10^{-4} D$, although shown to be sufficiently fine for flow problems with $Re_D = O(10^5)$, may have to be smaller for $Re_D = O(10^6)$ problems.

The flow solver and convergence levels are less of an issue in this case. The flow solver is well validated and the simulations were continued until the forces and moments had converged.

Boundary-layer transition is a formidable issue for high- α forebody flows as pointed out by Haines (Ref. 23). Even at the highest Reynolds number considered here, $Re_D = 2.1 \times 10^6$, small regions of laminar flow exist (particularly in the nose region) which can have a major impact on the global flow

development. Currently, there are no transition prediction schemes for 3-D RANS solvers and, hence, the accurate specification of transition onset becomes a tedious and time-consuming task. Transition prediction schemes have been successfully implemented for the solution of 2-D problems (e.g., Ref. 24). However, 3-D transition prediction is at least an order of magnitude more complicated than 2-D transition prediction.

The modeling of turbulence remains one of the most problematic areas of CFD-based force & moment prediction. In this study, the algebraic Baldwin-Lomax model and the one-equation Spalart-Allmaras model have been used. Based on the work of Murman & Chaderjian (Ref. 21) it was expected that the Spalart-Allmaras model would provide more accurate prediction of the forces & moments. However, this work shows the differences to be small. If anything, the Baldwin-Lomax based predictions agree slightly better with the experimental results. This is in agreement with the most recent observations by Murman (Ref. 25) who notes that the application of one- and two-equation turbulence models to high- α forebody flows with strong vortices outside the boundary layer leads to excessive levels of turbulent eddy-viscosity in these vortices. These high levels of eddy viscosity lead to a deterioration of the flow predictions. Murman (Ref. 25) suggests the use of a vortex filter that is Galilean-invariant and computationally efficient to improve the predictions based on the one- and two-equation turbulence models.

Conclusions

A Reynolds-averaged Navier-Stokes code, OVERFLOW, has been used to predict the rotary flow characteristics of two forebody models. This computational tool shows great promise for the analysis of major problems encountered in the application of the rotary-balance wind-tunnel test technique for aircraft dynamics including model support interference, wind-tunnel wall interference, and Reynolds number effects.

Future efforts will include additional simulations to further assess the effect of rotational speed and angle of attack on the forebody flow development and compare the results with those in the experimental database. Also, the effect of the sting on the flow development as well as the computed forces and moments will be assessed. Last but not least, we would like to evaluate ways to incorporate a 3-D transition prediction methodology in the flow solver.

Acknowledgements

The efforts of the first, second, and fourth author are supported by the NASA Langley Research Center under Grant No. NAG-1-2006 and Consortium Agreement NCC1-01-007. We would like to thank Dr. Roger Strawn of the Army/NASA Rotorcraft Division at the Ames Research Center, Dr. Pieter Buning of the NASA Langley Research Center, Dr. Earl Duque of Northern Arizona University, and Dr. Jasim Ahmad and Dr. Scott Murman of Elore, Inc. for their valuable help and suggestions during the various stages of this project.

References

1. Pauley, H., Ralston, J., and Dickes, E., "Experimental Study of the Effects of Reynolds Number on High Angle of Attack Aerodynamic Characteristics of Forebodies During Rotary Motion," NASA CR 195033, Jan. 1995.
2. Dunham, D.M., "Rotary Results on Forebody Models," Cooperative Programme on Dynamic Wind Tunnel Experiments for Manoeuvring Aircraft, AGARD AR-305, Oct. 1996, pp. 7-1-7-14.
3. Kandil, O.A., and Chuang, H.A., "Unsteady Navier-Stokes Computations Past Oscillating Delta Wing at High Incidence," AIAA Journal Vol. 28, No. 8, Sep. 1990, pp. 1565-1572.
4. Sturek, W.B., Nietubicz, C.J., Sahu, J., and Weinacht, P., "Applications of Computational Fluid Dynamics to the Aerodynamics of Army Projectiles," Journal of Spacecraft and Rockets, Vol. 31, No. 2, Mar-Apr. 1994, pp. 186-189.
5. Weinacht, P., and Sturek, W.B., "Computation of the Roll Characteristics of a Finned Projectile," Journal of Spacecraft and Rockets, Vol. 33, No. 6, Nov-Dec. 1996, pp. 769-775.

6. Weinacht, P., Sturek, W.B., and Schiff, L.B., "Navier-Stokes Predictions of Pitch Damping for Axisymmetric Projectiles," *Journal of Spacecraft and Rockets*, Vol. 34, No. 6, Nov-Dec. 1997, pp. 753-761.
7. Weinacht, P., "Navier-Stokes Predictions of the Individual Components of the Pitch-Damping Sum," *Journal of Spacecraft and Rockets*, Vol. 35, No. 5, Sep-Oct. 1998, pp. 598-605.
8. Chaderjian, N.M. and Schiff, L.B., "Numerical Simulation of Forced and Free-to-Roll Delta-Wing Motions," *Journal of Aircraft*, Vol. 33, No. 1, Jan-Feb. 1996, pp. 93-99.
9. Ahmad, J. and Duque, E.P.N., "Helicopter Rotor Blade Computation in Unsteady Flows Using Moving Overset Grids," *Journal of Aircraft*, Vol. 33, No. 1, Jan-Feb. 1996, pp. 54-60.
10. Limache, A.C., and Cliff, E.M., "Aerodynamic Sensitivity Theory for Rotary Stability Derivatives," *Journal of Aircraft*, Vol. 37, No. 4, July-Aug. 2000, pp. 676-683.
11. Park, M.A., and Green, L.L., "Steady-State Computation of Constant Rotational Rate Dynamic Stability Derivatives," AIAA Paper 2000-4321, Aug. 2000.
12. Buning, P.G., Jespersen, D.C., Pulliam, T.H., Chan, W.M., Slotnick, J.P., Krist, S.E., and Renze, K.J., "OVERFLOW User's Manual, Version 1.8," NASA Langley Research Center, Feb. 1998.
13. Meakin, R., "A New Method for Establishing Grid Communication Among Systems of Overset Grids," AIAA Paper 91-1586, June 1991.
14. Chen, C.L., McCroskey, W.J., and Obayashi, S., "Numerical Solutions of Forward-Flight Rotor Flow Using an Upwind Method," *Journal of Aircraft*, Vol. 28, No. 6, June 1991, pp. 374-380.
15. Srinivasan, G.R., Baeder, J.D., Obayashi, S., and McCroskey, W.J., "Flowfield of a Lifting Rotor in Hover: A Navier-Stokes Simulation," *AIAA Journal*, Vol. 30, No. 10, Oct. 1992, pp. 2371-2378.
16. Ahmad, J.U., "Higher Order Discretization of Convective Fluxes of Navier-Stokes Equations: Helicopter Computations," AIAA Paper 99-3226, June 1999.
17. Baldwin, B.S., and Lomax, H., "Thin Layer Approximation and Algebraic Model for Separated Turbulent Flows," AIAA Paper 78-257, Jan. 1978.
18. Spalart, P.R., and Allmaras, S.R., "A One-Equation Turbulence Model for Aerodynamic Flows," *La Recherche Aéronautique*, No. 1, 1994, pp. 5-21 (Also, AIAA Paper 92-0439, Jan. 1992).
19. Chan, W. M., "OVERGRID," Handbook of Grid Generation, J.F.Thompson, B.K. Soni and N.P. Weatherill (Eds.), CRC Press, 1999, pp. A-49 through A-50.
20. Chan, W. M., "Innovative Software Streamlines Overset Grid Generation," *NAS News*, Vol. 3, No. 3, May-June 1998.
21. Murman, S.M., and Chaderjian, N.M., "Application of Turbulence Models to Separated High-Angle-of-Attack Flows," AIAA Paper 98-4519, Aug. 1998.
22. Van Dam, C.P., "Recent Experience with Different Methods of Drag Prediction," *Progress in Aerospace Sciences*, Vol. 35, 1999, pp. 751-798.
23. Haines, A.B., "Scale Effects on Aircraft and Weapon Aerodynamics," AGARD AG-323, 1995.
24. Brodeur, R.R., and van Dam, C.P., "Transition Prediction for a Two-Dimensional Navier-Stokes Solver Applied to Wind-Turbine Airfoils," AIAA Paper 2000-0047, Jan. 2000.
25. Murman, S.M., "Vortex Filtering for Turbulence Models Applied to Crossflow Separation," AIAA Paper 2000-0114, Jan. 2001.

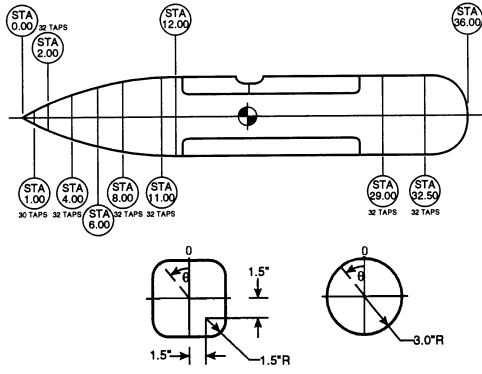


Fig. 1 Schematic of circular and square ogive models.

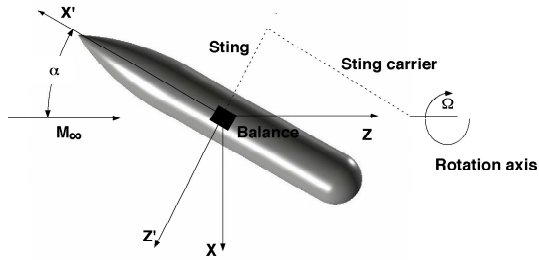
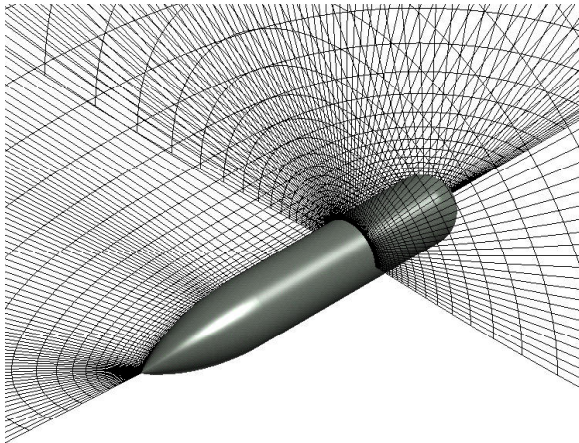
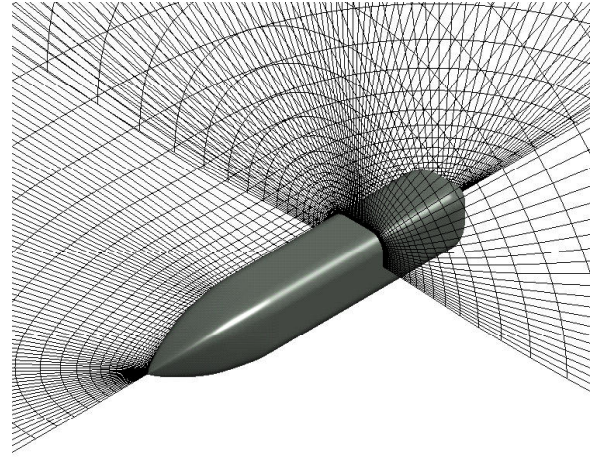


Fig. 2 Sketch depicting layout of rotary test of forebody models. Body-fixed axis system (X' , Y' , Z') is used in experiments and axis system (X , Y , Z) is used in numerical simulations. Neither the sting nor any other rotary-balance equipment is included in the computational model.



(a) Circular ogive



(b) Square ogive

Fig. 3. Close-up of volume grid for forebody model.

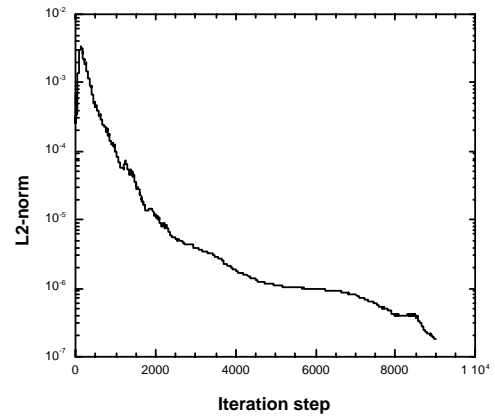


Fig. 4 Convergence characteristics for circular ogive at $\alpha = 60^\circ$, $Re_D = 2.08 \times 10^6$, $M_\infty = 0.21$, and $\Omega b / (2U_\infty) = -0.20$.

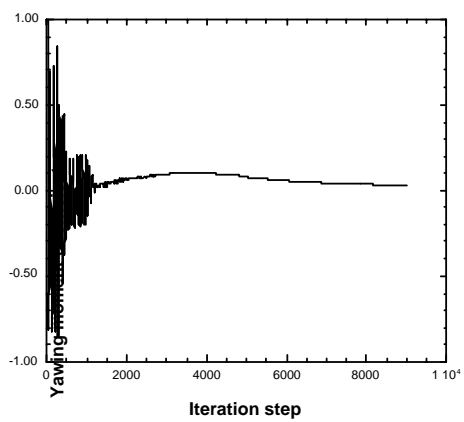
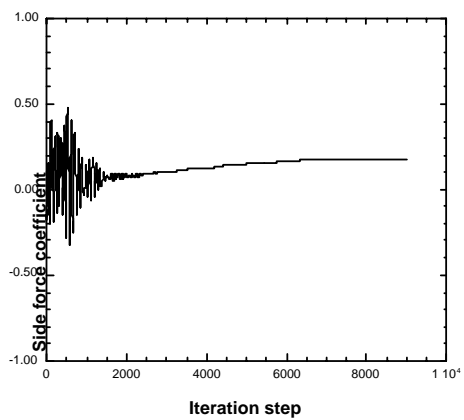
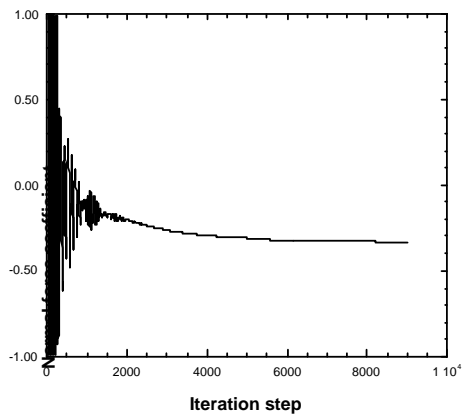
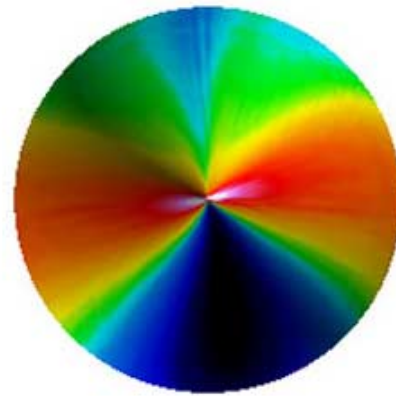
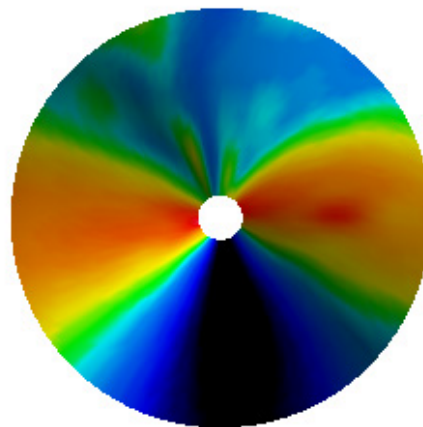
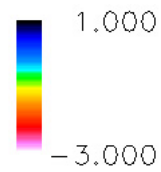


Fig. 5 Normal force, side force, and yawing moment predictions for circular ogive at $\alpha = 60^\circ$, $Re_D = 2.08 \times 10^6$, $M_\infty = 0.21$, and $\Omega b/(2U_\infty) = -0.20$.



(a) Computed



(b) Measured

Fig. 6 Measured and computed forebody pressure distributions for circular ogive at $\alpha = 60^\circ$, $Re_D = 2.08 \times 10^6$, $M_\infty = 0.21$, and $\Omega b/(2U_\infty) = -0.20$.

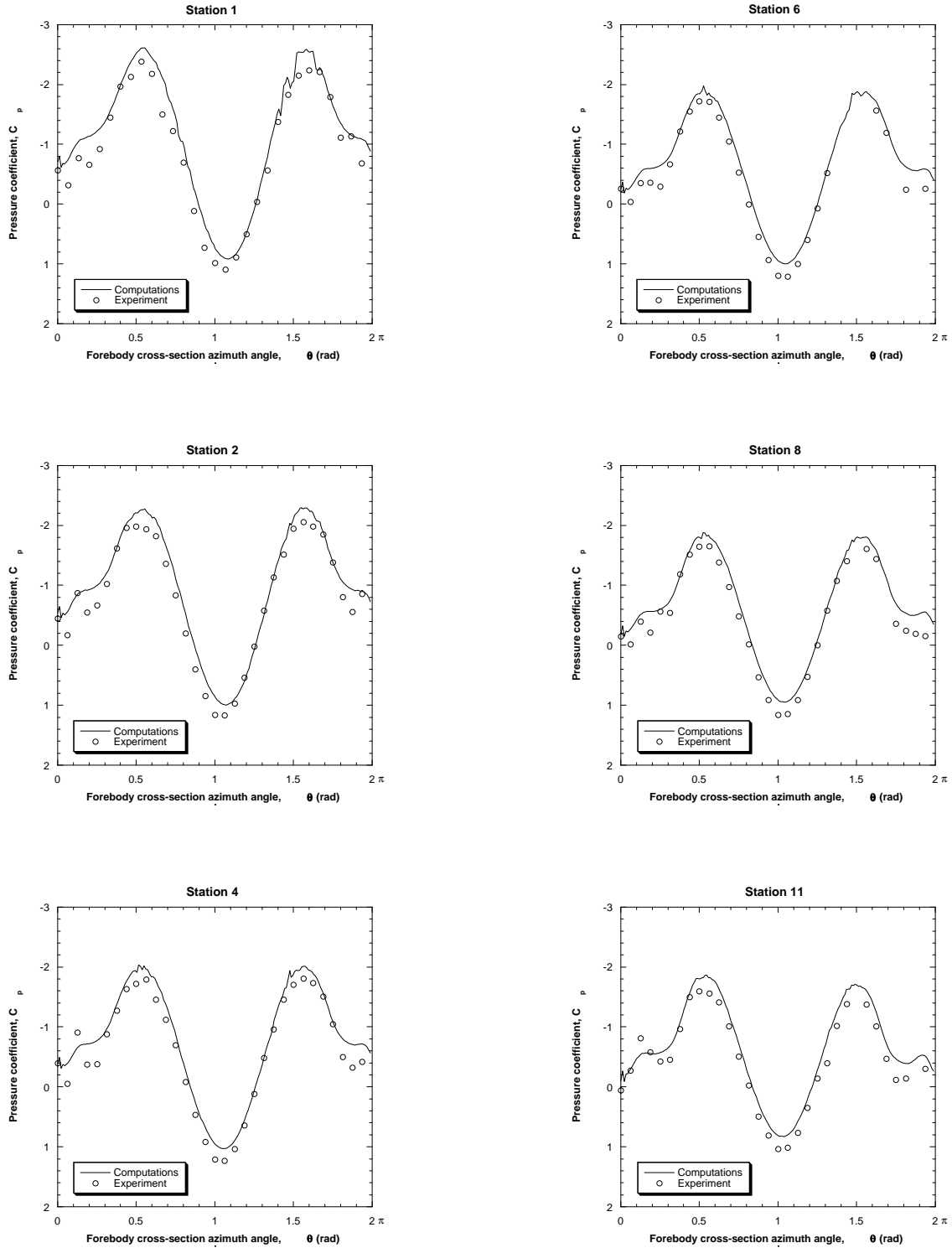
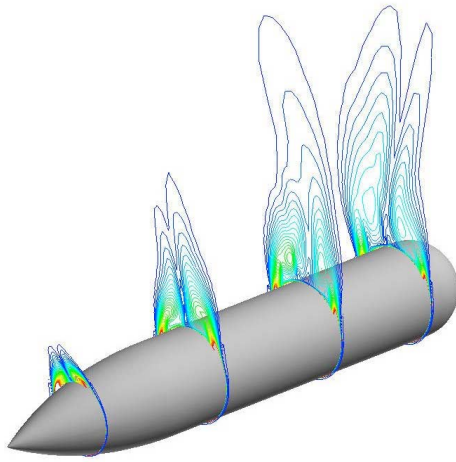
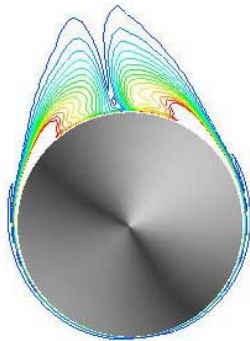


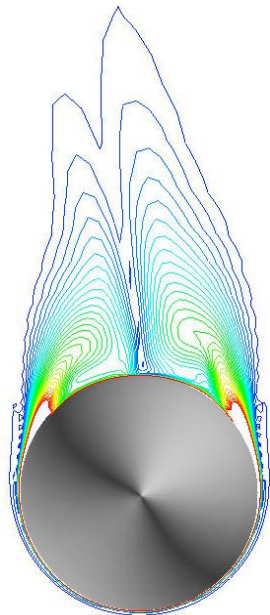
Fig. 7 Measured and computed forebody pressure distributions for circular ogive at $\alpha = 60^\circ$, $Re_D = 2.08 \times 10^6$, $M_\infty = 0.21$, and $\Omega b/(2U_\infty) = -0.20$. Stations as marked in Fig. 1.



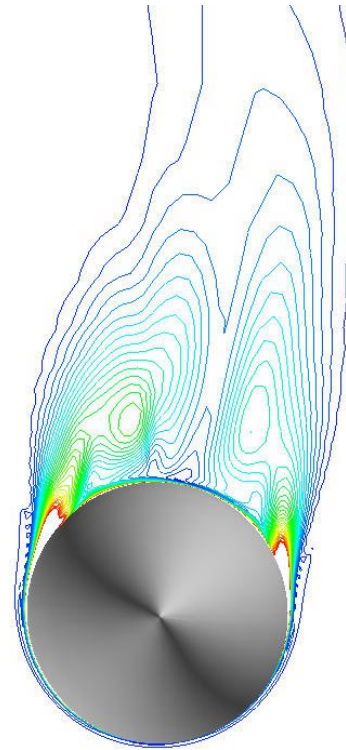
(a) Perspective view



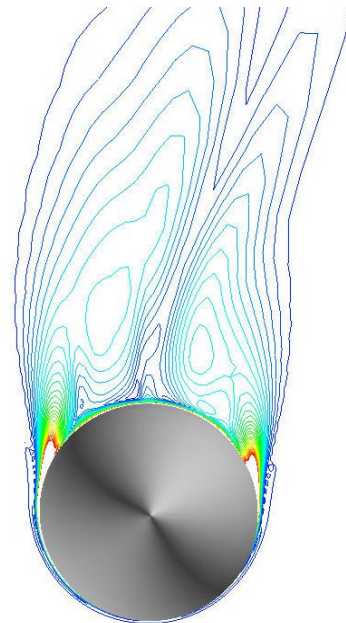
(b) Forebody station (40/130)



(c) Centerbody station (66/130)

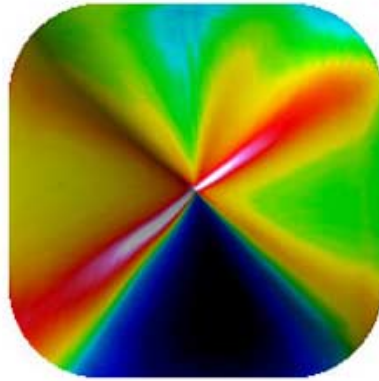


(d) Centerbody station (76/130)

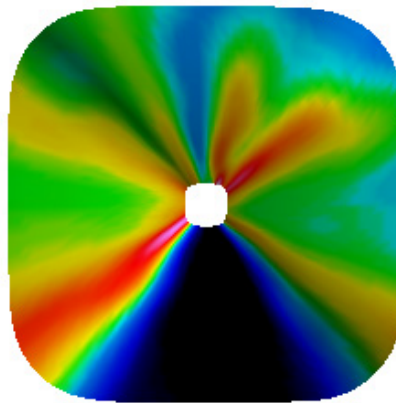


(e) Aftbody station (87/130)

Fig. 8 Axial vorticity contours for circular ogive at $\alpha = 60^\circ$, $Re_D = 2.08 \times 10^6$, $M_\infty = 0.21$, and $\Omega b/(2U_\infty) = -0.20$.



(a) Computed



(b) Measured

Fig. 9 Measured and computed forebody pressure distributions for square ogive at $\alpha = 60^\circ$, $Re_D = 2.09 \times 10^6$, $M_\infty = 0.21$, and $\Omega b/(2U_\infty) = -0.20$.

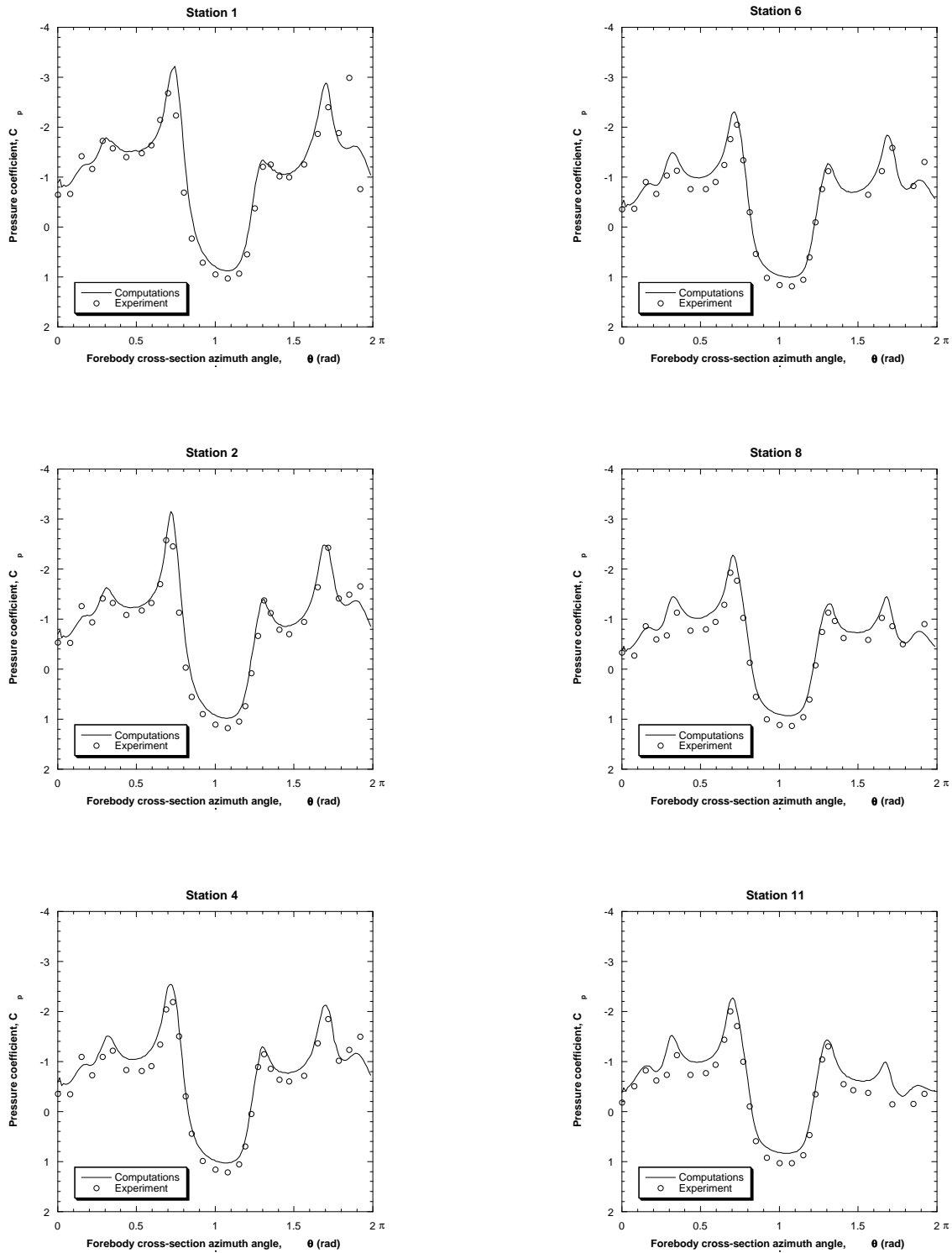


Fig. 10 Measured and computed forebody pressure distributions for square ogive at $\alpha = 60^\circ$, $Re_D = 2.09 \times 10^6$, $M_\infty = 0.21$, and $\Omega b/(2U_\infty) = -0.20$. Stations as marked in Fig. 1.

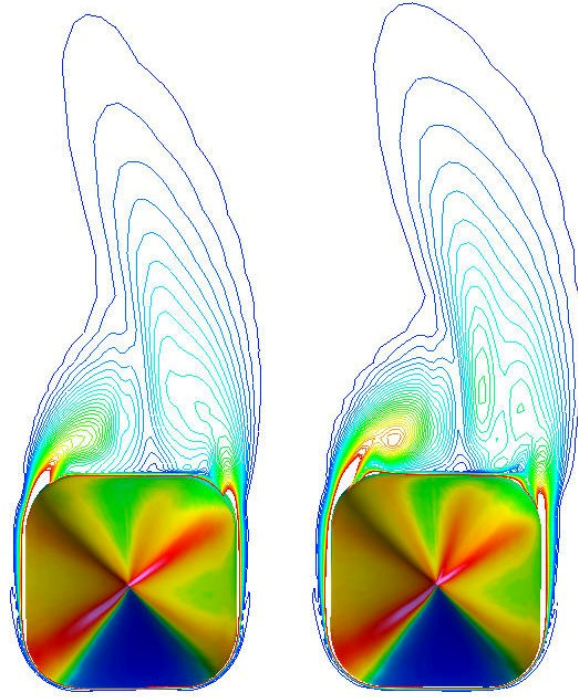


Fig. 11 Comparison between Baldwin-Lomax (left) and Spalart-Allmaras (right) solutions for square airfoil at $\alpha = 60^\circ$, $Re_D = 2.09 \times 10^6$, $M_\infty = 0.21$, and $\Omega b/(2U_\infty) = -0.20$.

Paper: 39

Author: Dr. Van Dam

Question by Dr. Radespiel: Does the experimental data at high Reynolds number indicate boundary layer transition on the forebody?

Answer: Unfortunately, the transition location was not determined during the rotary wind tunnel tests of the given forebody models. There is some limited data with boundary-layer trips on the forebody. However, it is not clear that transition really occurred at the trips.

This page has been deliberately left blank



Page intentionnellement blanche